Phosphomolybdic acid as efficient hole injection material in perovskite optoelectronic devices

Vahid Fallah Hamidabadi,[1,2] Cristina Momblona,[1] Daniel Perez-Del-Rey,[1] Ali Bahari,[2] Michele Sessolo[1] and Henk J. Bolink[1]

[1]Instituto de Ciencia Molecular, Universidad de Valencia, C/ J. Beltrán 2, 46980, Paterna, Spain.

[2]Department of Physics, Faculty of Basic Sciences, University of Mazandaran, Babolsar 47416-95447, Iran

[†]Electronic supplementary information (ESI) available: see DOI:

Abstract

Efficient perovskite devices consist in a perovskite film sandwiched in between charge selective layers, in order to avoid non-radiative recombination. A common metal oxide used as p-type or hole transport layer is molybdenum oxide. MoO_3 is of particular interest for its very large work function, which allows it to be used both as an interfacial charge transfer material as well as a dopant for organic semiconductors. However, high quality and high work function MoO_3 is typically thermally evaporated in vacuum. An alternative solution-processable high work function material is phosphomolybdic acid (PMA), which is stable, commercially available and environmentally friendly. In this communication, we show the first application of PMA in efficient vacuum processed perovskite devices. We found that the direct growth of perovskite films onto PMA lead to strong charge carrier recombination, hindering the solar cell photovoltage. By using an energetically suitable selective transport layer placed in between PMA and the perovskite film, solar cells with efficiency > 13% as well as LEDs with promising quantum efficiency can be obtained.

Organic-inorganic lead halide perovskites are being extensively investigated for applications in efficient thin-film solar cells[1-3] and, more recently, light-emitting diodes (LEDs).[4] Their success is due to the abundancy of the precursor compounds, ease of obtaining high quality perovskite thin-films by simple coating methods[5, 6] and to the unique set of physical properties, such as high absorption coefficient, long carrier recombination lifetime and defect tolerance,[7, 8] among others. In model perovskite absorbers such as methylammonium lead iodide (MAPI), free carriers are rapidly generated after light-absorption.[9] Hence, in order to limit charge recombination, efficient solar cells consist in a perovskite film sandwiched in between charge selective layers, typically organic or metal oxide semiconductors.[10, 11] Organic semiconductors are advantageous because there chemically tuned to fulfill specific properties (mobility, energetics), and can be processed at low temperature from solution or by sublimation. On the other hand, metal oxides are intrinsically more stable towards the environmental agents, and can strongly enhanced the stability of perovskite solar cells.[12-14] Common metal oxides used as p-type or hole transport layers (HTLs) are nickel oxide,[15, 16] tungsten oxide[17, 18] and molybdenum oxide.[19-21] The high work function of anode buffer layers is beneficial for the hole injection/extraction in LEDs or solar cells, as it allows to match the electrode work function with the HOMO of the hole transport material. An important example is the use of used a self-organized buffer layers consisting of poly(3,4-ethylenedioxythiophene):poly(styrenesulfonate) (PEDOT:PSS) and a perfluorinated polymeric acid, resulting in very large work function layers.[22-24] Within the inorganic materials, molybdenum trioxide is of particular interest for its very large work function, which allows it to be used both as an interfacial charge transfer material[25] as well as a dopant for organic semiconductors.[26] The latter property is the reason for its frequent use as an interlayer between an organic semiconductor and the electrode as it ensures an ohmic contact between the two.[27] Although MoO_3 can be solution-processed at mild temperature in the form of nanoparticles or when mixed with suitable reagents,[28-30] high quality and low work function MoO_3 is typically thermally evaporated in vacuum. An alternative solution-processable high work function material is phosphomolybdic acid (PMA), a polyoxometallate with a central phosphorous atom surrounded by twelve molybdenum oxyanions.[31] It is stable, commercially available and environmentally friendly, making it an interesting candidate as high work function interface in organic solar cells and LEDs.[32, 33] In this communication, we show the first application of PMA in efficient vacuum processed perovskite solar cells. We found that the direct growth of perovskite films onto PMA lead to strong charge

carrier recombination, hindering the solar cell photovoltage. By using an energetically suitable selective transport layer placed in between PMA and the perovskite film, solar cells with efficiency > 13% as well as LEDs with promising quantum efficiency can be obtained.

PMA was purchased from Sigma-Aldrich and used as received. The solution was diluted to 10 mg/mL and spin-coated onto indium tin oxide (ITO) coated glass substrates at 1500 rpm for 1 minute. The film thickness was approximately 10 nm, as determined by a mechanical profilometer. The film was annealed on a hot plate at 150 °C for 10 minutes in a nitrogen filled glove box, following a previously developed method.[32]

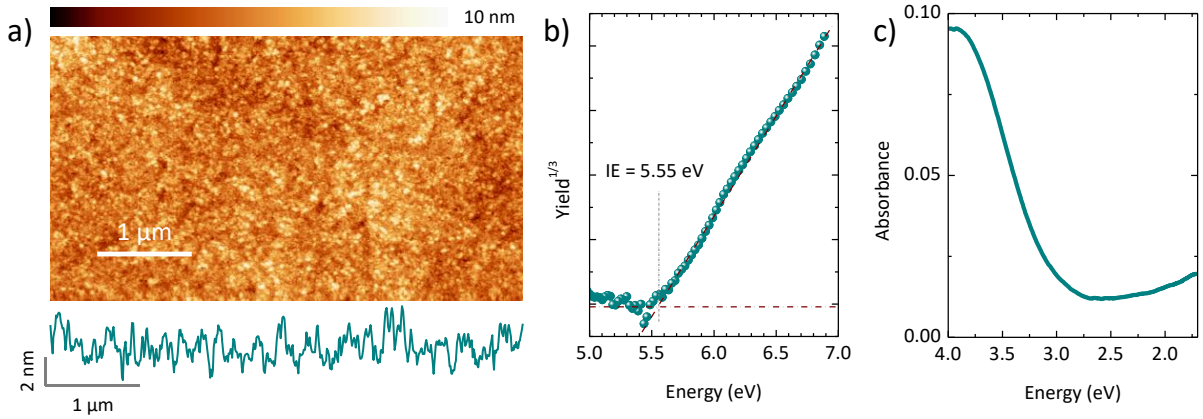

Fig. 1 (a) AFM Topography of the surface of PMA deposited onto ITO/glass substrate with (below) the corresponding cross-section. (b) UV photoemission spectrum in air of the same sample, showing an ionization potential of 5.55 eV. (c) UV-Vis absorption spectrum of a PMA film on glass. The absorption at low energy is due to optical interference.

The surface morphology was initially investigated by atomic force microscopy (AFM, Fig. 1a). We found a very flat and homogenous surface, with fine and compact aggregates resulting in a root-mean-square roughness R_{rms} as low as 1.1 nm, calculated over a 25 µm^2 area (for comparison, ITO has an R_{rms} typically < 3 nm[34]). A more significant quantification of the surface quality for optoelectronic devices is the peak-to-valley roughness R_{pv}, which directly correlates with the device leakage current.[35] Over the same area, the maximum observed R_{pv} was 10.6 nm, well below that of typical ITO substrates employed in most research type solar cells (> 50 nm). Apart from

the morphology, a key feature of the PMA is the large work function (ϕ), which makes it suitable as hole transport or injection layer (HTL and HIL, respectively). Hence we characterized the material by a combination of air photoemission spectroscopy and Kelvin Probe measurements. The absolute ionization potential (IE) of PMA was estimated by linear extrapolation of the cubic root of the photoemission (Fig. 1b), and was found to be 5.55 eV. We then measured by Kelvin Probe the contact potential difference (*CPD*) of the PMA/ITO substrate, obtaining a value of 0.383 ± 0.002 eV, respectively. The absolute PMA work function (ϕ_{PMA}) can be calculated taking into account the work function of the calibrated tip (ϕ_{tip} = 4.64 eV), as $\phi_{PMA} = \phi_{Tip} + CPD_{PMA}$ = 5.05 eV. Taking into account a bandgap of approximately 3 eV, estimated by the onset of the optical absorption (Fig. 1c), we can estimate the valence band maximum at -5.5 eV and the conduction band minimum at -2.5 eV from the vacuum level. We observed some differences as compared to literature data, which might be due to the different techniques used to estimate the electronic properties of the material.[33, 36] The large work function suggests the PMA to be slightly p-type, in accordance with previous reports.[32] In view of the favorable morphological and electronic characteristics of PMA, we used it as the substrate to prepare vacuum-processed perovskite solar cells, using methylammonium lead iodide (MAPI) as the thin-film absorber. The MAPI films were prepared by dual-source thermal vacuum deposition by controlling the sublimation rates of the methylammonium iodide (MAI) and PbI_2 precursors, as reported elsewhere.[37] The solar cells structure used (Fig. 2a) was ITO/PMA (10 nm)/MAPI (500 nm)/C_{60} (25 nm)/BCP (8 nm)/Ag (100 nm), where the fullerene C_{60} is the electron transport layer (ETL) and BCP is bathocuproine, a common electrode interlayer used in high efficiency solar cells.[38-40] All organic films and the reflecting metal were sublimed in vacuum chambers.

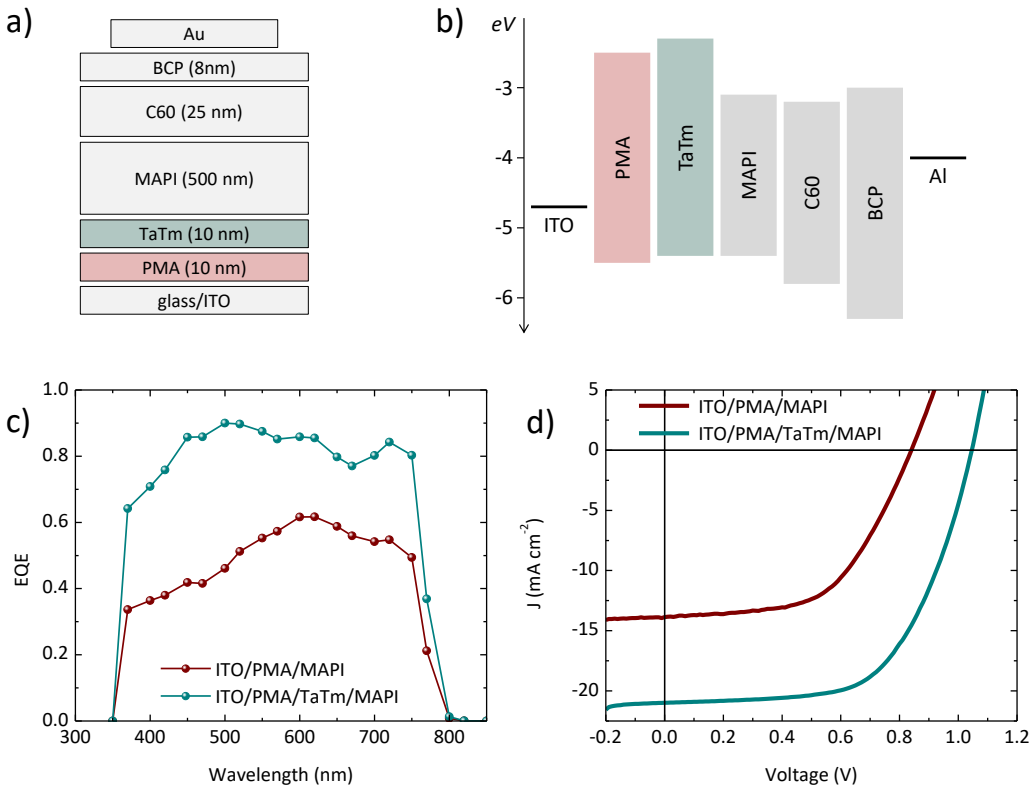

Fig. 2 (a) Schematics of the solar cells layout and (b) flat band energy diagram for the set of materials employed. (c) Photocurrent spectral response and (d) current density vs. voltage under 100 mW/cm^2 illumination for devices with and without the TaTm hole transport layer.

The solar cells were not encapsulated and were characterized in a nitrogen filled glove box. The solar cell with the PMA/MAPI interface showed a rather low spectral response, with the external quantum efficiency (EQE, Fig. 2b) going from about 0.35 at short wavelength to approximately 0.5-0.6 in the spectral range close to the bandgap of the perovskite. The EQE is low when considering the thickness of the perovskite film (500 nm), which should allow to quantitative harvest the photons with energy above the perovskite bandgap (1.6 eV). The reduced spectral response results in a low current density at short circuit (J_{sc}, 13.9 mA/cm^2), as observed by measuring the current density vs. voltage (J-V) curve under solar simulated illumination (Fig. 2c, photovoltaic parameters in Table 1). The current losses are likely associated with charge carrier recombination, as suggested by the low open circuit voltage (V_{oc}, 0.84 V) and fill factor (FF, 55.4%). Similar phenomena have been observed in perovskite solar cells where the MAPI was

directly vacuum processed onto the metal oxide.[41] In that case, a thin intrinsic charge selective layer was found beneficial for the device functioning, in particular to avoid charge recombination. Hence we prepared solar cells placing a thin layer of N4,N4,N4",N4"-tetra([1,1'-biphenyl]-4-yl)-[1,1':4',1"- terphenyl]-4,4"-diamine (TaTm, 10 nm) in between the PMA and the perovskite. The solar cell spectral response was found to substantially recover in the presence of TaTm, with EQE values in the range of 0.7-0.9 through the whole visible spectrum (Fig. 2b). As a consequence, the J_{sc} was substantially improved up to 20.9 mA/cm^2, which is comparable to state-of-the-art vacuum processed perovskite solar cells.[37, 40] The photovoltage was also recovered (1.05 V), as expected when the perovskite absorber is sandwiched between charge selective layers (TaTm and C60, in this case). The FF was slightly improved to 60.6%, resulting in a power conversion efficiency (PCE) of 13.3%.

Table 1 Photovoltaic parameters for solar cell under 100 mW/cm^2 illumination with and without the TaTm hole transport layer.

Hole collection interface	*J_{sc} (mA/cm^2)*	*V_{oc} (V)*	*FF (%)*	*PCE (%)*
ITO/PMA	13.9	0.84	55.4	6.5
ITO/PMA/TaTm	20.9	1.05	60.6	13.3

In order to investigate the origin of the marked differences among devices with or without the TaTm HTL in between PMA and the perovskite, we run extensive morphological, structural and optical characterization (Fig. S1). From the electron microscopy we could not observe any difference depending on the substrate used, and both MAPI films appear homogenous and compact, with grain size in the order of 100-300 nm. Also the optical absorption and the x-ray diffraction (XRD) patterns of perovskite films deposited on PMA and TaTm did not evidence a dependence on the substrate used (Fig. S1c-d). The absorbance in the visible range and the onset of the absorption are essentially equal. This and the XRD patterns, closely resembling the expected reference, suggest the formation of high quality polycrystalline MAPI films both on PMA and

TaTm. Hence the origin of the very different optoelectronic behavior is most likely to be found at the very interface between the perovskite absorber and the underlying functional film. It has been recently demonstrated how the mechanism of MAPI film formation is dependent on the chemical nature of the substrate (organic vs. metal oxide).[42, 43] Due to a catalytic activity of metal oxides, several organic byproducts are formed at the beginning of the deposition due to degradation of methylammonium iodide. This delays the perovskite crystallization and results in thin interfacial layer with a stoichiometry deviating from the expected one.[43] Such interfacial layer can be responsible of the strongly augmented charge recombination observed when our MAPI films are vacuum-deposited on PMA, whose chemical structure resembles the surface of a metal oxide. Besides the strong improvement observed upon insertion of TaTm, however, the PCE of the solar cells is still limited by the FF, which suggests a limited conductivity of the PMA film. On the other hand, the charge extraction appears to be excellent, as can be observed from the nearly flat current density at low bias. Hence, the PMA does lead to the formation of low barrier (ohmic) contacts between the TaTm and ITO electrode. This makes PMA an alternative to the recently presented p-type dopant interlayer in a similar configuration.

Finally, we also characterized the electroluminescence characteristics of the optimized device with ITO/PMA/TaTm hole injection interface. The device layout is the same as in Fig. 2a, and the electroluminescence can be measured by applying a forward bias while measuring the emitted photon flux as power density in an integrating sphere. The J-V curve (Fig. 3a) shows a low leakage current, indicative of a good quality diode, and a steep current injection starting at about 0.5 V. This fast rise in current density corroborates the before mentioned observation that PMA enables a very low barrier for charge transfer from the ITO electrode to the TaTm and subsequently the perovskite film. Electroluminescence was detected at bias as low as 1 V, and the power output increased rapidly until reaching approximately 2000 $\mu W/cm^2$. These parameters correspond to a maximum external quantum efficiency for electroluminescence (EQE_{EL}) of 0.06% (Fig. 3b). Such EQE_{EL} is approximately 1 order of magnitude lower as compared to state-of-the-art vacuum deposited solar cells,[37] indicating that non-radiative recombination is taking place, limiting the power output of the solar cells.

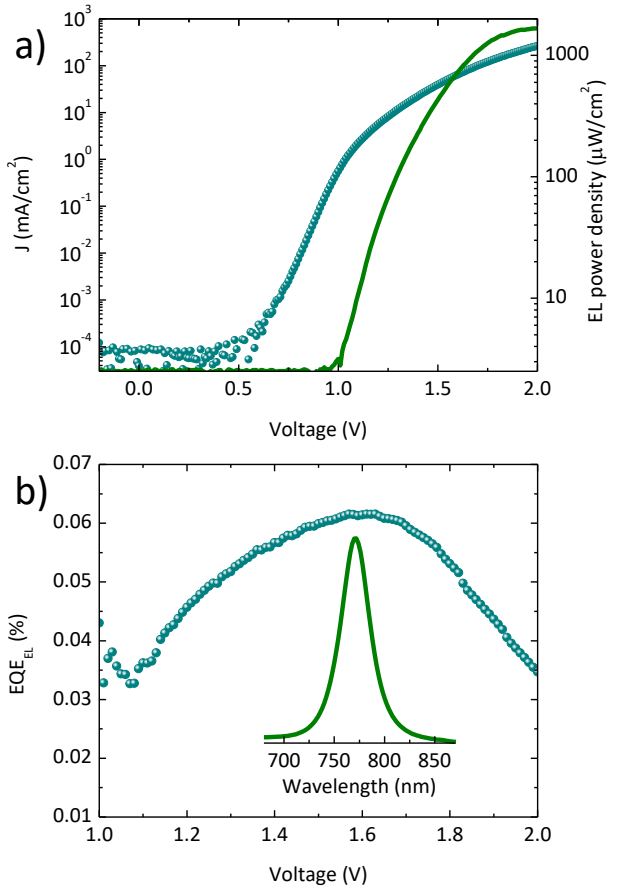

Fig. 3 (a) Current (symbols) and power (line) densities vs. applied bias for a solar cell with TaTm hole transport layer. (b) Corresponding EQE_{EL} vs. bias and (inset) electroluminescence spectrum of the device.

In summary, we have used phosphomolybdic acid (PMA) as an alternative solution-processed interlayer to enhance the hole extraction in perovskite solar cells. We characterized the morphology and energetics of the material, and employed to enhance carrier collection at the ITO/perovskite interface. We found that the direct growth of methylammonium lead iodide onto PMA leads to high carrier recombination, due to a different growth of the perovskite or to the lack of electron blocking effect, which is limiting the device efficiency. This phenomenon can be alleviated by inserting a selective charge transport layer (TaTm) on top of the PMA, resulting in high photovoltage solar cells. The PMA is a very effective interlayer for these p-i-n type solar cells, as it effectively removes the charge transfer barrier between the ITO electrode and the organic hole transporting layer. Due to this very low voltages are required for charge injection and

light emission when the diode is driven under forward bias. The solar cell performance appears to be limited by the conductivity of the PMA layer. This may be overcome by post-deposition treatments or doping strategies.[13, 18] However, here we have demonstrated the high potential of this simple solution processable hole injection layer.

Acknowledgements

We acknowledge financial support from the European Union H2020 project INFORM (grant 675867), the Spanish Ministry of Economy and Competitiveness (MINECO) via the Unidad de Excelencia María de Maeztu MDM-2015-0538, MAT2017-88821-R and the Generalitat Valenciana (Prometeo/2016/135). M.S. thanks the MINECO for his post-doctoral RyC contract.

References

1. N.-G. Park, M. Grätzel, T. Miyasaka, K. Zhu and K. Emery, *Nature Energy*, 2016, **1**, 16152.
2. W. Zhang, G. E. Eperon and H. J. Snaith, *Nature Energy*, 2016, **1**, 16048.
3. J.-P. Correa-Baena, M. Saliba, T. Buonassisi, M. Grätzel, A. Abate, W. Tress and A. Hagfeldt, *Science*, 2017, **358**, 739-744.
4. B. R. Sutherland and E. H. Sargent, *Nature Photonics*, 2016, **10**, 295.
5. J. Ávila, C. Momblona, P. P. Boix, M. Sessolo and H. J. Bolink, *Joule*, 2017, **1**, 431-442.
6. Z. Li, T. R. Klein, D. H. Kim, M. Yang, J. J. Berry, M. F. A. M. van Hest and K. Zhu, *Nature Reviews Materials*, 2018, **3**, 18017.
7. J. M. Ball and A. Petrozza, *Nature Energy*, 2016, **1**, 16149.
8. J. Huang, Y. Yuan, Y. Shao and Y. Yan, *Nature Reviews Materials*, 2017, **2**, 17042.
9. J. Shi, Y. Li, Y. Li, D. Li, Y. Luo, H. Wu and Q. Meng, *Joule*, 2018, **2**, 879-901.
10. A.-N. Cho and N.-G. Park, *ChemSusChem*, 2017, **10**, 3687-3704.
11. V. Zardetto, B. L. Williams, A. Perrotta, F. Di Giacomo, M. A. Verheijen, R. Andriessen, W. M. M. Kessels and M. Creatore, *Sustainable Energy & Fuels*, 2017, **1**, 30-55.
12. J. You, L. Meng, T.-B. Song, T.-F. Guo, Y. Yang, W.-H. Chang, Z. Hong, H. Chen, H. Zhou, Q. Chen, Y. Liu, N. De Marco and Y. Yang, *Nature Nanotechnology*, 2015, **11**, 75.
13. W. Chen, Y. Wu, Y. Yue, J. Liu, W. Zhang, X. Yang, H. Chen, E. Bi, I. Ashraful, M. Grätzel and L. Han, *Science*, 2015, **350**, 944-948.
14. K. O. Brinkmann, J. Zhao, N. Pourdavoud, T. Becker, T. Hu, S. Olthof, K. Meerholz, L. Hoffmann, T. Gahlmann, R. Heiderhoff, M. F. Oszajca, N. A. Luechinger, D. Rogalla, Y. Chen, B. Cheng and T. Riedl, *Nature Communications*, 2017, **8**, 13938.
15. J.-Y. Jeng, K.-C. Chen, T.-Y. Chiang, P.-Y. Lin, T.-D. Tsai, Y.-C. Chang, T.-F. Guo, P. Chen, T.-C. Wen and Y.-J. Hsu, *Advanced Materials*, 2014, **26**, 4107-4113.
16. J. H. Kim, P.-W. Liang, S. T. Williams, N. Cho, C.-C. Chueh, M. S. Glaz, D. S. Ginger and A. K.-Y. Jen, *Advanced Materials*, 2015, **27**, 695-701.

17. K. Wang, Y. Shi, Q. Dong, Y. Li, S. Wang, X. Yu, M. Wu and T. Ma, *The Journal of Physical Chemistry Letters*, 2015, **6**, 755-759.
18. Y. Hou, X. Du, S. Scheiner, D. P. McMeekin, Z. Wang, N. Li, M. S. Killian, H. Chen, M. Richter, I. Levchuk, N. Schrenker, E. Spiecker, T. Stubhan, N. A. Luechinger, A. Hirsch, P. Schmuki, H.-P. Steinrück, R. H. Fink, M. Halik, H. J. Snaith and C. J. Brabec, *Science*, 2017, **358**, 1192-1197.
19. E. Della Gaspera, Y. Peng, Q. Hou, L. Spiccia, U. Bach, J. J. Jasieniak and Y.-B. Cheng, *Nano Energy*, 2015, **13**, 249-257.
20. B.-S. Kim, T.-M. Kim, M.-S. Choi, H.-S. Shim and J.-J. Kim, *Organic Electronics*, 2015, **17**, 102-106.
21. J. Xu, O. Voznyy, R. Comin, X. Gong, G. Walters, M. Liu, P. Kanjanaboos, X. Lan and E. H. Sargent, *Advanced Materials*, 2016, **28**, 2807-2815.
22. Y.-H. Kim, H. Cho, J. H. Heo, T.-S. Kim, N. Myoung, C.-L. Lee, S. H. Im and T.-W. Lee, *Advanced Materials*, 2015, **27**, 1248-1254.
23. Y.-H. Kim, C. Wolf, H. Cho, S.-H. Jeong and T.-W. Lee, *Advanced Materials*, 2016, **28**, 734-741.
24. Y.-H. Kim, C. Wolf, Y.-T. Kim, H. Cho, W. Kwon, S. Do, A. Sadhanala, C. G. Park, S.-W. Rhee, S. H. Im, R. H. Friend and T.-W. Lee, *ACS Nano*, 2017, **11**, 6586-6593.
25. P. Schulz, J. O. Tiepelt, J. A. Christians, I. Levine, E. Edri, E. M. Sanehira, G. Hodes, D. Cahen and A. Kahn, *ACS Applied Materials & Interfaces*, 2016, **8**, 31491-31499.
26. M. Kröger, S. Hamwi, J. Meyer, T. Riedl, W. Kowalsky and A. Kahn, *Organic Electronics*, 2009, **10**, 932-938.
27. J. Meyer, S. Hamwi, M. Kröger, W. Kowalsky, T. Riedl and A. Kahn, *Advanced Materials*, 2012, **24**, 5408-5427.
28. Y.-J. Lee, J. Yi, G. F. Gao, H. Koerner, K. Park, J. Wang, K. Luo, R. A. Vaia and J. W. P. Hsu, *Advanced Energy Materials*, 2012, **2**, 1193-1197.
29. Y. Jiang, C. Li, H. Liu, R. Qin and H. Ma, *Journal of Materials Chemistry A*, 2016, **4**, 9958-9966.
30. Y.-H. Lou and Z.-K. Wang, *Nanoscale*, 2017, **9**, 13506-13514.
31. Y. Zhu, Z. Yuan, W. Cui, Z. Wu, Q. Sun, S. Wang, Z. Kang and B. Sun, *Journal of Materials Chemistry A*, 2014, **2**, 1436-1442.
32. S. Ohisa, S. Kagami, Y.-J. Pu, T. Chiba and J. Kido, *ACS Applied Materials & Interfaces*, 2016, **8**, 20946-20954.
33. G. Ji, Y. Wang, Q. Luo, K. Han, M. Xie, L. Zhang, N. Wu, J. Lin, S. Xiao, Y.-Q. Li, L.-Q. Luo and C.-Q. Ma, *ACS Applied Materials & Interfaces*, 2018, **10**, 943-954.
34. U. Betz, M. Kharrazi Olsson, J. Marthy, M. F. Escolá and F. Atamny, *Surf. Coat. Tech.*, 2006, **200**, 5751-5759.
35. K. B. Kim, Y. H. Tak, Y. S. Han, K. H. Baik, M. H. Yoon and M. H. Lee, *Jpn. J. Appl. Phys.*, 2003, **42**, L438-L440.
36. X. Jia, L. Shen, M. Yao, Y. Liu, W. Yu, W. Guo and S. Ruan, *ACS Applied Materials & Interfaces*, 2015, **7**, 5367-5372.
37. C. Momblona, L. Gil-Escrig, E. Bandiello, E. M. Hutter, M. Sessolo, K. Lederer, J. Blochwitz-Nimoth and H. J. Bolink, *Energy & Environmental Science*, 2016, **9**, 3456-3463.
38. P. Peumans, V. Bulovic and S. R. Forrest, *Applied Physics Letters*, 2000, **76**, 2650-2652.
39. Z. Xiao, C. Bi, Y. Shao, Q. Dong, Q. Wang, Y. Yuan, C. Wang, Y. Gao and J. Huang, *Energy & Environmental Science*, 2014, **7**, 2619-2623.
40. J. Avila, L. Gil-Escrig, P. P. Boix, M. Sessolo, S. Albrecht and H. J. Bolink, *Sustainable Energy & Fuels*, 2018, DOI: 10.1039/C8SE00218E.
41. D. Pérez-del-Rey, P. P. Boix, M. Sessolo, A. Hadipour and H. J. Bolink, *The Journal of Physical Chemistry Letters*, 2018, **9**, 1041-1046.
42. H. Xu, Y. Wu, J. Cui, C. Ni, F. Xu, J. Cai, F. Hong, Z. Fang, W. Wang, J. Zhu, L. Wang, R. Xu and F. Xu, *Physical Chemistry Chemical Physics*, 2016, **18**, 18607-18613.

43. S. Olthof and K. Meerholz, *Scientific Reports*, 2017, **7**, 40267.